HHS Public Access

Author manuscript

Sci Transl Med. Author manuscript; available in PMC 2024 July 16.

Published in final edited form as:

Sci Transl Med. 2024 June 19; 16(752): eadl5931. doi:10.1126/scitranslmed.adl5931.

Inhibiting AGTR1 reduces AML burden and protects the heart from cardiotoxicity in mouse models

Yi Pan[1,2,†], **Chen Wang**[1,2,†], **WenXuan Zhou**[1,2], **Yao Shi**[1,2], **XiaDuo Meng**[1,2], **Yasir Muhammad**[2,3], **Richard D. Hammer**[4], **Bei Jia**[5], **Hong Zheng**[5], **De-Pei Li**[1,6], **Zhenguo Liu**[1,6], **Gerhard Hildebrandt**[2,3], **XunLei Kang**[1,2,3,*]

[1]Center for Precision Medicine, Department of Medicine, University of Missouri School of Medicine, Columbia, MO 65212, USA.

[2]Ellis Fischel Cancer Center at MU Health Care, University of Missouri, Columbia, MO 65212, USA.

[3]Division of Hematology and Oncology, Department of Medicine, University of Missouri School of Medicine, Columbia, MO 65212, USA.

[4]Department of Pathology and Anatomical Sciences, University of Missouri School of Medicine, Columbia, MO 65212, USA.

[5]Division of Hematology/Oncology, Penn State University College of Medicine, Hershey, PA 17033, USA.

[6]Division of Cardiovascular Medicine, Department of Medicine, University of Missouri School of Medicine, Columbia, MO 65212, USA.

Abstract

Clinical treatment of acute myeloid leukemia (AML) largely relies on intensive chemotherapy. However, the application of chemotherapy is often hindered by cardiotoxicity. Patient sequence data revealed that angiotensin II receptor type 1 (*AGTR1*) is a shared target between AML and cardiovascular disease (CVD). We found that inhibiting AGTR1 sensitized AML to chemotherapy and protected the heart against chemotherapy-induced cardiotoxicity in a human AML cell–transplanted mouse model. These effects were regulated by the AGTR1-Notch1 axis in AML cells and cardiomyocytes from mice. In mouse cardiomyocytes, AGTR1 was hyperactivated by AML and chemotherapy. AML leukemogenesis increased the expression of the angiotensin-

*Corresponding author. kangxu@health.missouri.edu.

†These authors contributed equally to this work.

Author contributions: Y.P., C.W., and X.K. conceived the project, performed and designed the experiments, analyzed the results, and produced the figures. Y.P. and C.W. performed the bioinformatic and biostatistical analyses. W.Z., Y.S., and X.M. helped conduct in vitro tissue culture, Western blots, plasmid preparation, in vivo sample collection, and flow cytometry. Y.P. and C.W. performed the histological experiments. C.W. and W.Z. contributed to basic technical support such as cell sorting and flow cytometry. Y.P. prepared the NSG library and deep sequencing. Y.M. and G.H. acquired the clinical samples and managed the patient consent. B.J. and H.Z. helped with designing human-related experiments such as hAML sample transplantation. R.D.H, B.J., H.Z., D.-P.L., Z.L. Y.P., C.W., and X.K. made comments and suggestions on data quality and helped edit the draft of the manuscript. X.K. provided the funding. Y.P. and X.K. wrote the original draft. Y.P., C.W., X.K., and all other authors contributed to reviewing and editing.

Competing interests: G.H. is affiliated with Pfizer, Kite, a Gilead company, Incyte, Jazz Pharmaceuticals, Morphosys, Alexion Pharmaceuticals, Karyopharm Therapeutics, Seagen, Janssen, RAPA Therapeutics, Daichiy, Ono Pharmaceutical, AstraZeneca, CTI BioPharma Corp, Takeda, and Pharmacyclics. All other authors declare that they have no competing interests.

converting enzyme and led to increased production of angiotensin II, the ligand of AGTR1, in an MLL-AF9–driven AML mouse model. In this model, the AGTR1-Notch1 axis regulated a variety of genes involved with cell stemness and chemotherapy resistance. AML cell stemness was reduced after *Agtr1a* deletion in the mouse AML cell transplant model. Mechanistically, *Agtr1a* deletion decreased γ-secretase formation, which is required for transmembrane Notch1 cleavage and release of the Notch1 intracellular domain into the nucleus. Using multiomics, we identified AGTR1-Notch1 signaling downstream genes and found decreased binding between these gene sequences with Notch1 and chromatin enhancers, as well as increased binding with silencers. These findings describe an AML/CVD association that may be used to improve AML treatment.

INTRODUCTION

Acute myeloid leukemia (AML) and cardiovascular disease (CVD) are closely related. A high incidence of cardiac events has been observed in patients with AML, especially among those receiving intensive chemotherapy (1). AML and CVD can both be initiated by certain mutations in blood cells (2). Such close association suggests the existence of potential shared targets between AML and CVD that could be used to treat AML and protect cardiovascular function at the same time.

Angiotensin II receptor type 1 (AGTR1), the well-known CVD target, is responsible for cell proliferation, inflammation, and fibrosis (3). AGTR1 has also been reported to be associated with various solid tumor progressions, such as breast cancer and liver cancer (4, 5). In those cancers, AGTR1 inhibition resulted in decreased cancer cell proliferation, induction of apoptosis, and remodeling of the extracellular matrix (4, 5). However, AGTR1's role in hematological malignancies has not been well studied. Uz *et al.* (6) reported that an AGTR1 inhibitor (losartan) sensitized some leukemic cell lines to doxorubicin treatment. AGTR1-specific ligand angiotensin II was also found to act as an autocrine growth factor for AML and increase AML growth and colony-forming capacity in a dose-dependent manner (6, 7). As a result, we hypothesize that inhibition or knockout (KO) of AGTR1 suppresses AML development and protects the heart against cardiotoxicity.

RESULTS

AGTR1 is a shared factor between AML and CVD

To test the hypothesis that there are shared targets between AML and CVD, we analyzed whole-blood RNA sequencing (RNA-seq) data from the Cancer Genome Atlas–Acute Myeloid Leukemia (TCGA-LAML), BEATAML, Therapeutically Applicable Research to Generate Effective Treatments–Acute Myeloid Leukemia (TARGET-AML), and McCaffrey *et al.* (8). Unsupervised clustering was performed using Uniform Manifold Approximation and Projection (UMAP) to identify 12 clusters of patients with similar genetic expression (Fig. 1, A and B). Major overlaps were observed between patients with AML and patients with CVD in clusters 6, 7, and 8, highlighting patients sharing a similar genetic expression pattern (Fig. 1C). To explore what genes underscored clusters where AML and CVD coresided, we performed gene differential expression analysis to acquire differentially expressed genes (DEGs) [at least two fold change (FC) and $P < 0.05$] for each of clusters

6, 7, and 8, against clusters without AML/CVD overlap (Fig. 1, D and E). Furthermore, we acquired an AML gene set containing 358 genes and a CVD gene set containing 268 genes as summarized by harmonizome (9) and intersected these two gene sets with the above three DEG sets. This process yielded nine AML/CVD shared genes (*AGTR1*, *CXCL12*, *CD34*, *IL6*, *HLX*, *CAV1*, *ABCB1*, *TNF*, and *MEIS1*). *AGTR1* is a well-known regulator of CVD, and its role in AML has been understudied. We observed significantly higher expression of *AGTR1* in the blood cells of patients with AML compared with that of healthy controls in the BEATAML database (7.6-fold, $P = 6.294 \times 10^{-13}$; Fig. 1F). To further corroborate these results, we investigated the cell surface expression of *AGTR1* in 16 human AML (hAML) samples and 12 healthy human blood samples (Fig. 1, G and H), as well as total *AGTR1* mRNA expression (fig. S1, A and B). $CD34^+$ hAML stem cells (SCs) exhibited higher (5.4-fold) *AGTR1* expression compared with $CD34^+$ healthy controls, suggesting a specific enrichment of *AGTR1* in leukemic SC (LSC)–enriched AML cells (Fig. 1, G and H).

AGTR1 is essential for hAML development

We first generated three different short hairpin RNA (shRNAs) targeting *AGTR1* to functionally study the role of AGTR1 in hAML. All shRNAs efficiently decreased the total expression of AGTR1 and blocked the in vitro growth of multiple hAML cells, including *THP1*, *Kasumi1*, *MOLM*, *MV4–11*, and *NB4*. The one with the strongest knockdown (KD) effects (number 474) was carried on to the following experiments (fig. S2, A to D). We performed colony-forming unit (CFU) assays using primary specimens from 11 individuals with AML with high *AGTR1* expression compared with healthy control. Seven specimens could form essential colonies, of which shRNA effectively reduced *AGTR1* expression and reduced colony-forming ability (fig. S2, E and F). Next, we performed patient-derived xenograft experiments using *AGTR1*-KD and *AGTR1*-scramble hAML cells (Fig. 1I). Three hAML samples were successfully engrafted in nonobese diabetic/severe combined immunodeficient–interleukin-2 receptor subunit gamma (NSG) mice. Mice transplanted with *AGTR1*-KD hAML cells showed suppressed leukemia development as demonstrated by prolonged overall survival ($P < 0.001$) and reduced infiltration of green fluorescent protein $(GFP)^+$ cells (marking the lentivirus-infected hAML cells; $P < 0.001$) in hematopoietic organs (Fig. 1, J to P).

Hematopoietic cell–specific deletion of *Agtr1a* in mice does not affect normal hematopoiesis

We next generated a hematopoietic system–specific deletion of *Agtr1a* in mice to study its role in both normal hematopoiesis and AML development (10, 11). The $Agtr1a^{fl/fl}$:Vav-Cre^+ ($Agtr1a^{-/-}$; KO) mice displayed comparable lifespan to the control $Agtr1a^{fl/fl}$: Vav-Cre^- [$Agtr1a^{+/+}$; wild-type (WT)] mice, which is consistent with findings in the *Agtr1a* global KO mouse model (12). Furthermore, $Agtr1a^{-/-}$ mice have comparable frequency and numbers of hematopoietic stem and progenitor cells (HSPCs) [total of long-term hematopoietic SCs (LT-HSCs), short-term HSCs (ST-HSCs), and multiple potential progenitors (MPPs)] and downstream progenitor cells [including common myeloid progenitor, granulocyte-macrophage progenitor (GMP), and common lymphoid progenitor] in the bone marrow (BM) when compared with $Agtr1a^{+/+}$ mice (fig. S3, A to C) and regular cell cycle activity of HSCs (fig. S3, D and E). Functionally, AGTR1-deficient BM cells had comparable colony-

forming ability (fig. S3F) and engraftment ability with no biased lineage reconstitution (fig. S3, G and H) as WT BM cells.

Agtr1a KO in mice reduces leukemic burden and prolongs survival

We used two retrovirus transplantation mouse models to study the role of AGTR1 in the regulation of AML development. Lineage$^-$ (Lin$^-$) cells from *Agtr1a*$^{+/+}$ or *Agtr1a*$^{-/-}$ donor mice infected by the retroviral oncogene [MLL-AF9 (13) or AML1-ETO9a (14)]–internal ribosome entry site–GFP were used to induce AML as previously described (fig. S4A) (15–17). The recipient mice transplanted with MLL-AF9–transduced *Agtr1a*$^{-/-}$ AML cells (henceforth called *Agtr1a*$^{-/-}$ AML mice) developed leukemia slower than mice transplanted with *Agtr1a*$^{+/+}$ AML cells (on average, *Agtr1a*$^{-/-}$ AML mice survive 41.8 days versus *Agtr1a*$^{+/+}$ AML mice survive 32.2 days; $P = 0.004$) in primary transplantation (Fig. 2A). The delayed development of leukemia was correlated with 60.6, 59.2, 56.9, and 71.3% reductions in ratios of leukemia cells in different hematopoietic organs [Fig. 2B; $P < 0.01$ for the BM and $P < 0.001$ for the spleen, liver, and peripheral blood (PB)] and less infiltration of myeloid leukemia cells into the spleen, liver, and PB at 4 weeks after transplantation (Fig. 2, C to E) when compared with *Agtr1a*$^{-/-}$ AML mice. Similar results for survival and AML development were obtained in another mouse AML model using AML1-ETO9a–transformed AML cells (Fig. 2, F and G).

Agtr1a KO diminishes AML cell stemness by disturbing cell division

To determine the mechanisms by which AGTR1 regulates AML development, we analyzed genome-wide transcriptome changes in *Agtr1a*$^{+/+}$ versus *Agtr1a*$^{-/-}$ MLL-AF9 AML cells. This procedure yielded a gene expression signature consisting of 506 up-regulated and 1110 down-regulated genes (1.5 FC, $P < 0.05$). Genes associated with AML stemness and proliferation were down-regulated, and genes associated with cell cycle activity were inhibited in *Agtr1a*$^{-/-}$ AML (MSigDB, http://software.broadinstitute.org/gsea/msigdb/search.jsp; Fig. 2, H and I). Quantification of Hox gene expression, which are hallmarks of AML-SC self-renewal and maintenance, supported diminished stemness in AML (fig. S5A) (18). We then evaluated LSC markers in the BM of both MLL-AF9 and AML-ETO9a mice. At similar late AML development stages, there were fewer AML-SCs in the BM of *Agtr1a*$^{-/-}$ AML mice than in *Agtr1a*$^{+/+}$ AML mice (Fig. 2, J to L; $P < 0.001$). Next, we relied on functional assays to evaluate the activity of LSCs using serial CFU replating and secondary transplantation assays. We observed a reduction in self-renewal of AML-SCs as indicated by a stepwise reduction in the activity of *Agtr1a*$^{-/-}$ AML-SCs in CFU forming ability of 32.2, 50.1, and 59.9% upon serial plating (Fig. 2M). Moreover, secondary AML transplantation resulted in 2.8-fold ($P < 0.001$) prolonged survival than that of primary transplantation in *Agtr1a*$^{-/-}$ AML mice (Fig. 2, N and O, versus Fig. 2A).

In addition to the role of AGTR1 in supporting LSC activity, we investigated changes in the cell cycle of *Agtr1a*$^{-/-}$ AML mice at 6 weeks after transplantation (Fig. 2P and fig. S5B). We found that *Agtr1a*$^{-/-}$ BM had about fourfold more AML-SCs (49.5% versus 12.6%; $P < 0.001$) in the S phase and threefold (22.6% versus 68.2%; $P < 0.001$) fewer the G_2-M phase than did WT control BM (Fig. 2Q), highlighting cell cycle arrest at S phase. To assess potential DNA damage in the abnormally dividing AML cells, we examined the

phosphorylation of histone H2A histone family member X (H2AX) at Ser^{139}, a marker used to identify double-stranded DNA breaks during progression through the cell cycle. We found evidence of greater DNA damage in *Agtr1a*$^{-/-}$ AML cells than in their WT counterparts ($P < 0.001$) (Fig. 2, I, R, and S).

Rescued Notch1 abrogates impaired AML cell stemness and cell division induced by *Atgr1a* KO

To further understand the biological functions induced by *Agtr1a* KO, we performed leading-edge network analysis using the gene sets mentioned above (MSigDB; Fig. 3A). Analysis of these gene networks identified altered cell proliferation and immune response that are known to be induced by Notch1 signaling in human leukemia development (19). We observed down-regulation of the Notch1 pathway (Fig. 3B) and decreased expression of the Notch intracellular domain (NICD) in *Agtr1a*$^{-/-}$ AML cells (Fig. 3C). γ-Secretase is known to cleave transmembrane Notch1 and releases the NICD into the cytoplasm, which subsequently migrates into the nucleus and functions as a transcription factor (19). RNA expression of γ-secretase assemblies was not significantly altered (fig. S6A). As a result, to determine whether the decreased activation of Notch1 after *Agtr1a* KO is mediated by γ-secretase, we performed immunoprecipitation using Notch1 antibody to pull down cytoplasmic γ-secretase. We found less binding between γ-secretase and Notch1 after *Agtr1a* KO (Fig. 3D; $P < 0.001$), indicating that AGTR1 regulates Notch1 activity through γ-secretase activity. To confirm that *Agtr1a* inhibition affects AML development through the regulation of Notch1, we performed a rescue assay using the cell-transplanted mouse model. Notch1 was reintroduced into *Agtr1a*$^{-/-}$ MLL-AF9 mouse AML cells (Fig. 3E), which were used for the CFU assay and transplanted into recipient mice. Phenotypes associated with *Agtr1a* deletion, including mouse survival after secondary transplantation (Fig. 3F), leukemic burden (percentage of GFP^+ cells in the PB) (Fig. 3G), AML stemness (colony forming ability) (Fig. 3H), and AML cell cycle (S phase arrest) (Fig. 3, I and J, and fig. S6B), were rescued by Notch1 overexpression.

AGTR1-Notch1 signaling regulates three-dimensional genomic structure of chemoresistance genes

Recent studies have highlighted the crucial role of three-dimensional (3D) genomic structure changes in AML development, necessitating a deeper understanding of the underlying mechanisms (20). We observed alterations in histone modification gene signatures between *Agtr1a*$^{+/+}$ and *Agtr1a*$^{-/-}$ AML cells (Fig. 4A), aligning with the well-established role of Notch1 in chromatin structure regulation (19). To elucidate the mechanism by which AGTR1-Notch1 signaling influences AML development, we conducted in situ Hi-C and CUT&RUN assays of histone 3 lysine 27 acetylation (H3K27ac), histone 3 lysine 27 trimethylation (H3K27me3), and Notch1 using primary AML cells from *Agtr1a* WT and KO mice. Figure 4 (B and C) illustrates a region containing all the epigenetic data in the *Agtr1a*$^{+/+}$ and *Agtr1a*$^{-/-}$ AML mouse. Our analysis revealed A/B compartment changes in chromosomes 2, 6, and 17 induced by *Agtr1a* depletion (Fig. 4D). Furthermore, the most enriched differential binding sites of Notch1, H3K27ac, and H3K27me3 were observed in chromosome 2 (Fig. 4E). Subsequently, we identified 26 top differentially binding genes (DBGs) shared among H3K27ac, Notch1, and H3K27me3 (Fig. 4F and fig. S7A). Almost

a quarter of these top DBGs have been associated with chemotherapy resistance (*Il2ra, Hmcn2, St8sia6, Rasgrp1, Prkcp,* and *Dpp4*; Fig. 4G). In WT AML cells, each of those genes formed a loop with co-occurring enhancers downstream or upstream. However, such loops were absent in *Agtr1a*$^{-/-}$ AML cells.

An AGTR1 inhibitor simultaneously sensitizes AML to chemotherapy and relieves chemotherapy-induced cardiotoxicity

We next investigated the combination effects of AML chemotherapy (AraC) and an AGTR1 inhibitor (losartan) in mouse models of AML. We xenografted primary hAML cells into NSG mice. After confirming the engraftment by measuring percentages of hCD45 cells in PB 4 weeks after transplantation, mice were randomized to receive phosphate-buffered saline (PBS) (200 μl, once daily), AraC (50 mg/kg, once a day, 5 days), losartan (10 mg/kg, once daily), or combination therapy (AraC + losartan, A + L) (fig. S8A). Overall survival and the ratio of hAML cells in the PB at weeks 4 and 8 were recorded. Whereas AraC or losartan alone reduced hAML burden and prolonged survival, the combination of AraC and losartan yielded the highest effects among all treated groups (Fig. 5, A to C; $P < 0.001$).

We next extended our investigation to explore the effect on heart function of AML mice. Left ventricular ejection fraction (LVEF), serum troponin, and serum B-type natriuretic peptide (BNP) were measured at weeks 4 and 8 after transplantation. LVEF was decreased ($P = 0.058$), and serum troponin and serum BNP were increased ($P < 0.05$) in PBS mice (Fig. 5, D to G), indicating AML-induced cardiotoxicity. Treatment with chemotherapy (AraC) further worsened these phenotypes, and the addition losartan abolished AML- or AML/AraC-induced cardiotoxicity. Mice were euthanized at weeks 4 and 8 to harvest hearts for evaluation of histological changes and expression amounts of RNA and protein. PBS mice showed increased cardiomyocyte size ($P < 0.05$), suggesting activation of angiotensin II–AGTR1 signaling (21, 22). However, treatment of AraC reduced cardiomyocyte size (Fig. 5, H and I; $P < 0.001$). Consistent with preserved cardiac contractility, the addition of losartan to PBS mice or AraC mice normalized cardiomyocyte size (Fig. 5, H and I; $P < 0.001$). Furthermore, cardiac apoptosis and myocardial collagen deposition, as shown by cleaved caspase-9 immunofluorescence assay and trichrome staining, were less abundant with the addition of losartan (Fig. 5, J to M; $P < 0.001$).

AGTR1 activation associates AML- and chemotherapy-induced cardiomyocyte toxicity

We next analyzed CVD-related signaling among mouse HSPCs on day 0, day 5, and day 28 after MLL-AF9 transformation. We observed a progressive increase in genes within the angiotensin pathway from day 0 to day 28 (Fig. 6A). Examining angiotensin-associated genes, we found increased expression of angiotensin-converting enzyme (*Ace*) on AML cells compared with normal blood cells (Fig. 6, B and C; $P < 0.001$). Mitogen-activated protein kinase (MAPK), c-Jun N-terminal kinase (JNK), and epidermal growth factor receptor (EGFR) pathways are known to be activated by AGTR1 activation (23). Along with increased angiotensin II in mouse serum (Fig. 6D and fig. S9A) and up-regulated angiotensin signaling activation in patients with AML (fig. S1B), we also observed increased expression of genes in these pathways in cardiomyocytes of AML mice (Fig. 6E). Furthermore, AraC increased AGTR1 signaling on cardiomyocytes in hAML-transplanted

mice (Fig. 6F). Likely, alteration of angiotensin II–AGTR1 signaling was observed in human cardiomyocytes treated with doxorubicin (Fig. 6G). We found increased NICD in the hearts of hAML mice (treated as fig. S8A) treated with PBS and AraC at week 8 versus week 4, suggesting Notch1 pathwa y activation. Such activation was abolished by losartan treatment (Fig. 6H).

DISCUSSION

In the present study, we have identified a shared target between AML and CVD and shed light on the interplay between them. We found that targeting AGTR1 suppressed AML development and protected cardiovascular function against cardiotoxicity induced by AML and chemotherapy. This is regulated by the AGTR1-Notch1 axis (fig. S9C). In AML, Notch1 functions as a transcription factor and regulates a variety of genes associated with stemness and chemoresistance.

AGTR1 is an important factor of the renin-angiotensin system, which is involved in the development and progression of a wide range of solid tumors (4, 5). Renin-angiotensin system components are expressed in tumor microenvironments, such as in endothelial cells, fibroblasts, and macrophages (24). As a result, inhibition of AGTR1 may disrupt the tumor microenvironment and, thus, inhibit tumor growth (25, 26). The underlying mechanism includes desmoplasia-mediated vessel compression, vascular endothelial growth factor–induced vessel leakiness and abnormal morphology, angiotensin II–mediated vasoconstriction of host vessels, proinflammatory cytokine production, and reactive oxygen species (ROS) generation. Inhibition of AGTR1 reduces these entities, increasing tumor oxygenation and reducing tumor immunosuppression and evasion (25, 26). AGTR1 inhibition also reduces the production of several proinflammatory cytokines, including transforming growth factor–β (TGF-β), interleukin-1α (IL-1α), IL-1β, IL-6, and IL-8, which induce immunosuppression, in either tumor or tumor microenvironment cells (24–28). ROS, generated by tumor cells and stromal cells to reduce T cell fitness and promote regulatory T cells and tumor-associated macrophage function, is also reduced by AGTR1 inhibition (28, 29). For example, Wu *et al.* (28) have shown in NF2 schwannoma that AGTR1 inhibition with losartan reduced the production of inflammatory factors, such as IL-1, IL-1β, CCL1, CCL4, and ROS, by tumor cells and inhibited IL-6/signal transducers and activators of transcription 3 and Toll-like receptor 4 signaling in tumor-associated macrophages, demonstrating the multifactorial role that AGTR1 play in solid tumors (24–29).

Likewise, the AML microenvironment, or AML niche, shares many similar characteristics with solid tumor microenvironments, including immune evasion and suppression, and vascular remodeling (30, 31). Our data have shown altered immune response and vascular regulation after *AGTR1* deletion, suggesting disturbed AML niche in the therapeutic benefits of targeting *AGTR1*. This direction is worth further investigation.

Whereas AGTR1 was also reported to regulate Notch1 activity through γ-secretase in other tissues, no study has demonstrated the exact mechanism that AGTR1 affects γ-secretase activity (32, 33). However, there are several indications pointing toward possible

explanations. AGTR1 activation is widely recognized for triggering the activation of specific transcription factors, such as nuclear factor κB, and adenosine 3′,5′-monophosphate response element–binding protein, both of which are found in the PS1 promoter and are implicated in PS1 gene expression (34–36). In addition, angiotensin II activates various members of the MAPK pathway, which are linked to increased γ-secretase activity (34). Liu *et al.* (37) reported that AGTR1 affects γ-secretase complex formation through PS1 endo-cleavage. The transcriptomics analysis in our study showed that γ-secretase assemblies, *Pen2* (Psenen), *APH-1* (Aph1a), Nicastrin (Ncstn), and Presenelin 1 (*Psen1*), are minimally altered (fig. S6A). These facts suggest that AGTR1 is likely to affect γ-secretase activity at the posttranslational level instead of the expression level.

Targeting AGTR1 diminishes chemotherapy-induced cardiotoxicity through the shared signaling pathway as in AML (AGTR1-Notch1). This is consistent with our initial hypothesis that AGTR1 is a shared target between AML and CVD. We observed that AML chemotherapy activates the AGTR1-Notch1 axis. Standard 7 + 3 AML chemotherapy consists of AraC and doxorubicin. Whereas both AraC and doxorubicin are associated with DNA intercalation and doxorubicin is thought to cause cardiotoxicity by inducing necrosis and apoptosis of cardiomyocytes, the mechanism of AraC-induced cardiotoxicity is not clear (38, 39).

AML is associated with increased cardiac events, indicating that AML itself poses stress on the heart (1). Although malignant transformation–conferred inflammatory factor increase is suggested for impaired cardiac function in patients with AML, no specific mechanism was reported (40). We have shown that such stress is mediated by increased ACE expression upon malignant transformation. ACE is responsible for converting angiotensin I to angiotensin II, which subsequently activates AGTR1. Prior studies have also found increased *ACE* expression in patients with AML compared with healthy individuals (41, 42). Increased *ACE* expression is accompanied by increased AGTR1 ligand, angiotensin II, which influences malignancy (41, 42). Angiotensin II was found to increase AML growth and colony-forming capacity in a dose-dependent manner (6, 7).

In the heart, Notch signaling was reported to be responsible for myocardial and vascular remodeling induced by AGTR1 activation (43, 44). However, the mechanism of how Notch1 inhibition protects the heart from cardiotoxicity is not clear. Prior studies suggest that Notch1 activation and inhibition were both important for heart function, but chronic activation prevents cardiac progenitor cell differentiation (45–47). In the context of chronic activation, Notch1 inhibition preserves cardiac function by reducing cardiac fibrosis and enhancing cardiac reprogramming (47). Further study is warranted to investigate the mechanism of cardiotoxicity induced by AML and chemotherapy.

Our study has several limitations. The limited databases of blood RNA sequences of patients with CVD resulted in a difference between the numbers of patients with AML and patients with CVD included in the target discovery analysis. Including more patients with CVD may uncover more AML-CVD targets and improve clinical therapy. In addition, some mouse or rat AGTR1 antibodies were reported to be unspecific and unreliable (48). As a result, we validated our findings at the RNA level, and our experiments used human AGTR1

antibodies. In addition, the nonspecific antibodies have been discontinued and replaced by newer versions. AGTR1 antibodies are now KO-validated, including the antibody used in our study (ABclonal, A4140).

Mouse models of leukemia also differ from human disease in several ways, including differences in the immune system, BM microenvironment, and responses to treatments. Although we incorporated AML cells from patients with AML, the mouse models were immunodeficient. In addition, the onset and progression of leukemia in mice are often more rapid and less heterogeneous than in humans, potentially oversimplifying the disease's complexity. These differences necessitate careful interpretation of mouse data and validation of findings in human studies to ensure translational relevance.

In conclusion, our study identified that losartan, a commercially available drug that reduces AML development and enhances chemotherapy, protects against chemotherapy-induced cardiotoxicity. However, further studies are warranted to translate this work to patients, including investigating losartan's efficacy in heterogeneous human leukemia and investigating the differences in the BM microenvironment. Using humanized mouse models, advanced in vitro systems, and strategic early-phase clinical trials can help bridge these gaps to enhance translational success.

METHODS

Study design

This study aimed to investigate the therapeutic effects of AGTR1 inhibition on the simultaneous treatment of AML and cardiomyocyte toxicity. Human PB samples and cord blood samples (Institutional Review Board #2091050MU), and primary hAML samples (Institutional Review Board #2019932) were obtained at the University of Missouri Hospital. Written informed consent was obtained from all patients to use their blood samples for research purposes. Diagnosis of AML was confirmed by a pathologist using BM aspiration and biopsy and cytochemical and immunohistochemical tests. All mice were cared for in accordance with National Institutes of Health guidelines. Mouse experiments were planned to provide 80% power for a target effect size of 1.2 to 1.5 (effect size = |mean difference|/SD). All mice were randomly allocated into experimental groups. For all other experiments, at least two independent biological replicates were performed and used in the sample calculation. No data were excluded from the studies. The investigators were not blinded to the allocation of animals during the experiments and outcome assessment. All procedures were approved in advance by the Institutional Animal Care and Use Committee of the University of Missouri (#39322). We first analyzed *AGTR1* RNA and protein expression in AML cells compared with healthy control blood cells. We then evaluated the effect of AGTR1 inhibition or KO on human or mouse AML cells and on normal hematopoietic stem/progenitor cells in mice. We also performed multiomics to investigate the mechanisms of *Agtr1a* KO on mouse AML development. Detailed below are all criteria for experimental cutoffs, such as mouse end point censure, number of cells used, and statistical tests used.

Identifying related genes between AML and CVD

Patients with AML and patients with CVD RNA-seq data were obtained from TCGA-LAML, BEATAML, TARGET-AML, and McCaffery *et al.* (8). RNA-seq counts were normalized into reads per kilobase per million mapped reads (RPKM) and loaded into Seurat with each gene as a row and each patient as a column in R (49). Loaded data were integrated using individuals who were in a matched biological state ("anchors") to correct for technical differences between datasets (batch effect correction) and to perform comparative single-patient RNA-seq analysis across different conditions. DEGs between clusters were identified with the Wilcoxon rank sum test using the inherit FindMarkers function in Seurat. AML- and CVD-related genes were collected from harmonizome (9). The identified DEGs and AML- and CVD-related genes were intersected to obtain the core bond genes.

Mice

C57BL/6N, CD45.2, and CD45.1 mice were purchased from Charles River Inc. *Agtr1a*^{tm1Uky}/J mice were obtained from the Jackson Laboratory (stock #016211). The offspring were then crossed with Vav-iCre mice (stock #018968, the Jackson Laboratory) (11) to obtain *Agtr1a*$^{fl/fl}$:Vav-Cre mice. Reagents will be made available through a material transfer agreement.

Leukemia characterization

We performed the procedure as previously described (17). After transplantation, we monitored the survival; examined the size and histological properties of the BM, spleen, and liver; and analyzed the numbers and infiltration of leukemia cells in the PB, BM, spleen, and liver. Complete blood counts in PB were measured using a Hemavet 950FS. We also characterized different populations of leukemia cells using flow cytometry. Leukemia characterization was performed by investigators blinded to the experimental groups. Moribund leukemic mice were euthanized, and the time was recorded as the time of death. Mice that died for reasons unrelated to leukemia within 10 days after transplantation were excluded from the data analysis.

CUT&RUN

CUT&RUN was performed using CUT&RUN Assay Kit (Cell Signaling Technologies, #86652) according to the manufacturer's instructions. Briefly, cells were harvested, washed, and bound to activate concanavalin A–coated magnetic beads and permeabilize. The bead-cell complex was incubated overnight with the Notch1 (Cell Signaling Technologies, #3608), H3K27ac (Cell Signaling Technologies, #D5), or H3K27me3 (Cell Signaling Technologies, #C36B11) antibody at 4°C. Cells were washed three times and resuspended in 100 μl of protein A and G/micrococcal nuclease and incubated for 1 hour at room temperature. DNA fragments were isolated by phenol/chloroform extraction followed by ethanol precipitation. CUT&RUN libraries were prepared using the DNA library prep kit for Illumina systems (Cell Signaling Technologies, #56795) according to the manufacturer's instructions. Library quality was assessed using a TapeStation 4200 (Agilent). Sequencing was performed on an Illumina NovaSeq platform in 150–base pair paired-end mode.

Echocardiography

For the evaluation of cardiac function, mice were anesthetized with 1% isoflurane and analyzed with a Vevo 3100 High Resolution Imaging System (Visual Sonics Inc.) equipped with a 30-MHz probe (MS550D) (Visual Sonics). Echocardiographic parameters were measured under the long-axis M-mode when heart rate was about 450 beats/min. LVEF was calculated as previously described (dividing the stoke volume by the end-diastolic volume) (50).

Statistical analysis

Statistical analysis was performed using GraphPad Prism version 9.0 (GraphPad) or R. For comparison of two groups, we used Student's *t* test and when comparing three or more groups, and one-way or two-way analysis of variance (ANOVA) was used with Fisher's test for post hoc analyses. The survival rates of the two groups were analyzed using a log-rank test and were considered statistically significant if $P < 0.05$.

Supplementary Material

Refer to Web version on PubMed Central for supplementary material.

Acknowledgments:

We thank faculty members of the Center for Precision Medicine for discussion and suggestions.

Funding:

This work was funded by the National Cancer Institute (grant R37CA241603 to X.K.), the American Heart Association (grant 19CDA34770036 to X.K.), and the American Cancer Society (grant RSG-23-1152630 to X.K.).

Data and materials availability:

All data associated with this study are present in the paper or Supplementary Materials. The TCGA-LAML datasets analyzed are available in the UCSC Xena Browser (https://xena.ucsc.edu), or raw counts can be accessed through the GDC data portal (https://portal.gdc.cancer.gov; accession number phs000178). BEATAML raw counts can be accessed through Zenodo (10.5281/zenodo.11254158). All sequence datasets generated in the current study have been deposited in NCBI SRA database with the bioproject ID PRJNA1021980. Codes used to analyze data are available at Zenodo (doi: 10.5281/zenodo.11254158). shRNA vectors and modified cell lines are available upon request through material transfer agreements with X.K. of University of Missouri, USA.

REFERENCES AND NOTES

1. Kang Y, Assuncao BL, Denduluri S, McCurdy S, Luger S, Lefebvre B, Carver J, Scherrer-Crosbie M, Symptomatic heart failure in acute leukemia patients treated with anthracyclines. JACC CardioOncol. 1, 208–217 (2019). [PubMed: 32905430]
2. Calvillo-Arguelles O, Schoffel A, Capo-Chichi JM, Abdel-Qadir H, Schuh A, Carrillo-Estrada M, Liu S, Gupta V, Schimmer AD, Yee K, Shlush LI, Natarajan P, Thavendiranathan P, Cardiovascular disease among patients with AML and CHIP-related mutations. JACC CardioOncol. 4, 38–49 (2022). [PubMed: 35492819]

3. Forrester SJ, Booz GW, Sigmund CD, Coffman TM, Kawai T, Rizzo V, Scalia R, Eguchi S, Angiotensin II signal transduction: An update on mechanisms of physiology and pathophysiology. Physiol. Rev. 98, 1627–1738 (2018). [PubMed: 29873596]
4. Arrieta O, Villarreal-Garza C, Vizcaino G, Pineda B, Hernandez-Pedro N, Guevara-Salazar P, Wegman-Ostrosky T, Villanueva-Rodriguez G, Gamboa-Dominguez A, Association between AT1 and AT2 angiotensin II receptor expression with cell proliferation and angiogenesis in operable breast cancer. Tumour Biol. 36, 5627–5634 (2015). [PubMed: 25682288]
5. Shimomoto T, Ohmori H, Luo Y, Chihara Y, Denda A, Sasahira T, Tatsumoto N, Fujii K, Kuniyasu H, Diabetes-associated angiotensin activation enhances liver metastasis of colon cancer. Clin. Exp. Metastasis 29, 915–925 (2012). [PubMed: 22552372]
6. Uz B, Tatonyan SC, Sayitoglu M, Erbilgin Y, Ng OH, Buyukasik Y, Sayinalp N, Aksu S, Goker H, Ozcebe OI, Ozbek U, Haznedaroglu IC, Local hematopoietic renin-angiotensin system in myeloid versus lymphoid hematological neoplastic disorders. J. Renin Angiotensin Aldosterone Syst. 14, 308–314 (2013). [PubMed: 23132846]
7. Brunetde la Grange P, Ivanovic Z, Leprivey-Lorgeot V, Praloran V, Angiotensin II that reduces the colony-forming ability of hematopoietic progenitors in serum free medium has an inverse effect in serum-supplemented medium. Stem Cells 20, 269–271 (2002). [PubMed: 12004086]
8. McCaffrey TA, Toma I, Yang Z, Katz R, Reiner J, Mazhari R, Shah P, Tackett M, Jones D, Jepson T, Falk Z, Wargodsky R, Shtakalo D, Antonets D, Ertle J, Kim JH, Lai Y, Arslan Z, Aledort E, Alfaraidy M, Laurent III GS, RNA sequencing of blood in coronary artery disease: Involvement of regulatory T cell imbalance. BMC Med. Genomics 14, 216 (2021). [PubMed: 34479557]
9. Rouillard AD, Gundersen GW, Fernandez NF, Wang Z, Monteiro CD, McDermott MG, Ma'ayan A, The harmonizome: A collection of processed datasets gathered to serve and mine knowledge about genes and proteins. Database (Oxford) 2016, baw100 (2016). [PubMed: 27374120]
10. Rateri DL, Moorleghen JJ, Balakrishnan A, Owens III AP, Howatt DA, Subramanian V, Poduri A, Charnigo R, Cassis LA, Daugherty A, Endothelial cell-specific deficiency of Ang II type 1a receptors attenuates Ang II-induced ascending aortic aneurysms in LDL receptor$^{-/-}$ mice. Circ. Res. 108, 574–581 (2011). [PubMed: 21252156]
11. de Boer J, Williams A, Skavdis G, Harker N, Coles M, Tolaini M, Norton T, Williams K, Roderick K, Potocnik AJ, Kioussis D, Transgenic mice with hematopoietic and lymphoid specific expression of Cre. Eur. J. Immunol. 33, 314–325 (2003). [PubMed: 12548562]
12. Ito M, Oliverio MI, Mannon PJ, Best CF, Maeda N, Smithies O, Coffman TM, Regulation of blood pressure by the type 1A angiotensin II receptor gene. Proc. Natl. Acad. Sci. U.S.A. 92, 3521–3525 (1995). [PubMed: 7724593]
13. Krivtsov AV, Twomey D, Feng Z, Stubbs MC, Wang Y, Faber J, Levine JE, Wang J, Hahn WC, Gilliland DG, Golub TR, Armstrong SA, Transformation from committed progenitor to leukaemia stem cell initiated by MLL-AF9. Nature 442, 818–822 (2006). [PubMed: 16862118]
14. Yan M, Kanbe E, Peterson LF, Boyapati A, Miao Y, Wang Y, Chen IM, Chen Z, Rowley JD, Willman CL, Zhang DE, A previously unidentified alternatively spliced isoform of t(8;21) transcript promotes leukemogenesis. Nat. Med. 12, 945–949 (2006). [PubMed: 16892037]
15. Wang C, Nistala R, Cao M, Pan Y, Behrens M, Doll D, Hammer RD, Nistala P, Chang HM, Yeh ETH, Kang X, Dipeptidylpeptidase 4 promotes survival and stemness of acute myeloid leukemia stem cells. Cell Rep. 42, 112105 (2023). [PubMed: 36807138]
16. Kang X, Lu Z, Cui C, Deng M, Fan Y, Dong B, Han X, Xie F, Tyner JW, Coligan JE, Collins RH, Xiao X, You MJ, Zhang CC, The ITIM-containing receptor LAIR1 is essential for acute myeloid leukaemia development. Nat. Cell Biol. 17, 665–677 (2015). [PubMed: 25915125]
17. Kang X, Cui C, Wang C, Wu G, Chen H, Lu Z, Chen X, Wang L, Huang J, Geng H, Zhao M, Chen Z, Muschen M, Wang HY, Zhang CC, CAMKs support development of acute myeloid leukemia. J. Hematol. Oncol. 11, 30 (2018). [PubMed: 29482582]
18. Bhatlekar S, Fields JZ, Boman BM, Role of HOX genes in stem cell differentiation and cancer. Stem Cells Int. 2018, 1–15 (2018).
19. Aster JC, Pear WS, Blacklow SC, Notch signaling in leukemia. Annu. Rev. Pathol. 3, 587–613 (2008). [PubMed: 18039126]

20. Xu J, Song F, Lyu H, Kobayashi M, Zhang B, Zhao Z, Hou Y, Wang X, Luan Y, Jia B, Stasiak L, Wong JH, Wang Q, Jin Q, Jin Q, Fu Y, Yang H, Hardison RC, Dovat S, Platanias LC, Diao Y, Yang Y, Yamada T, Viny AD, Levine RL, Claxton D, Broach JR, Zheng H, Yue F, Subtype-specific 3D genome alteration in acute myeloid leukaemia. Nature 611, 387–398 (2022). [PubMed: 36289338]
21. Paradis P, Dali-Youcef N, Paradis FW, Thibault G, Nemer M, Overexpression of angiotensin II type I receptor in cardiomyocytes induces cardiac hypertrophy and remodeling. Proc. Natl. Acad. Sci. U.S.A. 97, 931–936 (2000). [PubMed: 10639182]
22. Kajstura J, Cigola E, Malhotra A, Li P, Cheng W, Meggs LG, Anversa P, Angiotensin II induces apoptosis of adult ventricular myocytes in vitro. J. Mol. Cell. Cardiol. 29, 859–870 (1997). [PubMed: 9152847]
23. Saito Y, Berk BC, Angiotensin II-mediated signal transduction pathways. Curr. Hypertens. Rep. 4, 167–171 (2002). [PubMed: 11884273]
24. Pinter M, Jain RK, Targeting the renin-angiotensin system to improve cancer treatment: Implications for immunotherapy. Sci. Transl. Med. 9, eaan5616 (2017). [PubMed: 28978752]
25. Kosugi M, Miyajima A, Kikuchi E, Horiguchi Y, Murai M, Angiotensin II type 1 receptor antagonist candesartan as an angiogenic inhibitor in a xenograft model of bladder cancer. Clin. Cancer Res. 12, 2888–2893 (2006). [PubMed: 16675585]
26. Yoshiji H, Kuriyama S, Kawata M, Yoshii J, Ikenaka Y, Noguchi R, Nakatani T, Tsujinoue H, Fukui H, The angiotensin-I-converting enzyme inhibitor perindopril suppresses tumor growth and angiogenesis: Possible role of the vascular endothelial growth factor. Clin. Cancer Res. 7, 1073–1078 (2001). [PubMed: 11309359]
27. Okazaki M, Fushida S, Harada S, Tsukada T, Kinoshita J, Oyama K, Tajima H, Ninomiya I, Fujimura T, Ohta T, The angiotensin II type 1 receptor blocker candesartan suppresses proliferation and fibrosis in gastric cancer. Cancer Lett. 355, 46–53 (2014). [PubMed: 25224569]
28. Wu L, Vasilijic S, Sun Y, Chen J, Landegger LD, Zhang Y, Zhou W, Ren J, Early S, Yin Z, Ho WW, Zhang N, Gao X, Lee GY, Datta M, Sagers JE, Brown A, Muzikansky A, Stemmer-Rachamimov A, Zhang L, Plotkin SR, Jain RK, Stankovic KM, Xu L, Losartan prevents tumor-induced hearing loss and augments radiation efficacy in NF2 schwannoma rodent models. Sci. Transl. Med. 13, eabd4816 (2021). [PubMed: 34261799]
29. Ugel S, De Sanctis F, Mandruzzato S, Bronte V, Tumor-induced myeloid deviation: When myeloid-derived suppressor cells meet tumor-associated macrophages. J. Clin. Invest. 125, 3365–3376 (2015). [PubMed: 26325033]
30. Taghiloo S, Asgarian-Omran H, Immune evasion mechanisms in acute myeloid leukemia: A focus on immune checkpoint pathways. Crit. Rev. Oncol. Hematol. 157, 103164 (2021). [PubMed: 33271388]
31. Duarte D, Hawkins ED, Akinduro O, Ang H, De Filippo K, Kong IY, Haltalli M, Ruivo N, Straszkowski L, Vervoort SJ, McLean C, Weber TS, Khorshed R, Pirillo C, Wei A, Ramasamy SK, Kusumbe AP, Duffy K, Adams RH, Purton LE, Carlin LM, Lo Celso C, Inhibition of endosteal vascular niche remodeling rescues hematopoietic stem cell loss in AML. Cell Stem Cell 22, 64–77.e6 (2018). [PubMed: 29276143]
32. Zhu D, Shi J, Zhang Y, Wang B, Liu W, Chen Z, Tong Q, Central angiotensin II stimulation promotes β amyloid production in Sprague Dawley rats. PLOS ONE 6, e16037 (2011). [PubMed: 21297982]
33. Ozasa Y, Akazawa H, Qin Y, Tateno K, Ito K, Kudo-Sakamoto Y, Yano M, Yabumoto C, Naito AT, Oka T, Lee JK, Minamino T, Nagai T, Kobayashi Y, Komuro I, Notch activation mediates angiotensin II-induced vascular remodeling by promoting the proliferation and migration of vascular smooth muscle cells. Hypertens. Res. 36, 859–865 (2013). [PubMed: 23719127]
34. Kuo LH, Hu MK, Hsu WM, Tung YT, Wang BJ, Tsai WW, Yen CT, Liao YF, Tumor necrosis factor-α-elicited stimulation of γ-secretase is mediated by c-Jun N-terminal kinase-dependent phosphorylation of presenilin and nicastrin. Mol. Biol. Cell 19, 4201–4212 (2008). [PubMed: 18667537]
35. Arumugam TV, Cheng YL, Choi Y, Choi YH, Yang S, Yun YK, Park JS, Yang DK, Thundyil J, Gelderblom M, Karamyan VT, Tang SC, Chan SL, Magnus T, Sobey CG, Jo DG, Evidence that γ-secretase-mediated Notch signaling induces neuronal cell death via the nuclear factor-kappaB-

Bcl-2-interacting mediator of cell death pathway in ischemic stroke. Mol. Pharmacol. 80, 23–31 (2011). [PubMed: 21450930]

36. McAllister-Lucas LM, Ruland J, Siu K, Jin X, Gu S, Kim DS, Kuffa P, Kohrt D, Mak TW, Nunez G, Lucas PC, CARMA3/Bcl10/MALT1-dependent NF-kappaB activation mediates angiotensin II-responsive inflammatory signaling in nonimmune cells. Proc. Natl. Acad. Sci. U.S.A. 104, 139–144 (2007). [PubMed: 17101977]
37. Liu J, Liu S, Matsumoto Y, Murakami S, Sugakawa Y, Kami A, Tanabe C, Maeda T, Michikawa M, Komano H, Zou K, Angiotensin type 1a receptor deficiency decreases amyloid β-protein generation and ameliorates brain amyloid pathology. Sci. Rep. 5, 12059 (2015). [PubMed: 26154270]
38. Wayangankar SA, Patel BC, Parekh HD, Holter JL, Lazzara R, High-dose cytosine arabinoside-induced symptomatic bradycardia. J. Cardiovasc. Med. 16 (suppl. 1), S38–S41 (2015).
39. Bloom MW, Hamo CE, Cardinale D, Ky B, Nohria A, Baer L, Skopicki H, Lenihan DJ, Gheorghiade M, Lyon AR, Butler J, Cancer therapy-related cardiac dysfunction and heart failure: Part 1: Definitions, pathophysiology, risk factors, and imaging. Circ. Heart Fail. 9, e002661 (2016). [PubMed: 26747861]
40. Getz KD, Sung L, Ky B, Gerbing RB, Leger KJ, Leahy AB, Sack L, Woods WG, Alonzo T, Gamis A, Aplenc R, Occurrence of treatment-related cardiotoxicity and its impact on outcomes among children treated in the AAML0531 clinical trial: A report from the children's oncology group. J. Clin. Oncol. 37, 12–21 (2019). [PubMed: 30379624]
41. Sinka L, Biasch K, Khazaal I, Peault B, Tavian M, Angiotensin-converting enzyme (CD143) specifies emerging lympho-hematopoietic progenitors in the human embryo. Blood 119, 3712–3723 (2012). [PubMed: 22282502]
42. Beyazit Y, Aksu S, Haznedaroglu IC, Kekilli M, Misirlioglu M, Tuncer S, Karakaya J, Koca E, Buyukasik Y, Sayinalp N, Goker H, Overexpression of the local bone marrow renin-angiotensin system in acute myeloid leukemia. J. Natl. Med. Assoc. 99, 57–63 (2007). [PubMed: 17304969]
43. de la Pompa JL, Epstein JA, Coordinating tissue interactions: Notch signaling in cardiac development and disease. Dev. Cell 22, 244–254 (2012). [PubMed: 22340493]
44. Rivera-Torres J, Guzman-Martinez G, Villa-Bellosta R, Orbe J, Gonzalez-Gomez C, Serrano M, Diez J, Andres V, Maraver A, Targeting γ-secretases protect against angiotensin II-induced cardiac hypertrophy. J. Hypertens. 33, 843–850 (2015). [PubMed: 25915889]
45. Gude N, Joyo E, Toko H, Quijada P, Villanueva M, Hariharan N, Sacchi V, Truffa S, Joyo A, Voelkers M, Alvarez R, Sussman MA, Notch activation enhances lineage commitment and protective signaling in cardiac progenitor cells. Basic Res. Cardiol. 110, 29 (2015). [PubMed: 25893875]
46. Nemir M, Croquelois A, Pedrazzini T, Radtke F, Induction of cardiogenesis in embryonic stem cells via downregulation of Notch1 signaling. Circ. Res. 98, 1471–1478 (2006). [PubMed: 16690879]
47. Nemir M, Kay M, Maison D, Berthonneche C, Sarre A, Plaisance I, Pedrazzini T, Inhibition of the NOTCH1 pathway in the stressed heart limits fibrosis and promotes recruitment of non-myocyte cells into the cardiomyocyte fate. J. Cardiovasc. Dev. Dis. 9, 111 (2022). [PubMed: 35448087]
48. Herrera M, Sparks MA, Alfonso-Pecchio AR, Harrison-Bernard LM, Coffman TM, Lack of specificity of commercial antibodies leads to misidentification of angiotensin type 1 receptor protein. Hypertension 61, 253–258 (2013). [PubMed: 23150519]
49. Hao Y, Hao S, Andersen-Nissen E, Mauck III WM, Zheng S, Butler A, Lee MJ, Wilk AJ, Darby C, Zager M, Hoffman P, Stoeckius M, Papalexi E, Mimitou EP, Jain J, Srivastava A, Stuart T, Fleming LM, Yeung B, Rogers AJ, McElrath JM, Blish CA, Gottardo R, Smibert P, Satija R, Integrated analysis of multimodal single-cell data. Cell 184, 3573–3587.e29 (2021). [PubMed: 34062119]
50. Lindsey ML, Kassiri Z, Virag JAI, de Castro Bras LE, Scherrer-Crosbie M, Guidelines for measuring cardiac physiology in mice. Am. J. Physiol. Heart Circ. Physiol. 314, H733–H752 (2018). [PubMed: 29351456]
51. Schwach V, Slaats RH, Cofino-Fabres C, Ten Den SA, Rivera-Arbelaez JM, Dannenberg M, van Boheemen C, Ribeiro MC, van der Zanden SY, Nollet EE, van der Velden J, Neefjes J, Cao L,

Passier R, A safety screening platform for individualized cardiotoxicity assessment. iScience 27, 109139 (2024). [PubMed: 38384853]

52. Wang C, Nistala R, Cao M, Li DP, Pan Y, Golzy M, Cui Y, Liu Z, Kang X, Repair of limb ischemia is dependent on hematopoietic stem cell specific-SHP-1 regulation of TGF-β1. Arterioscler. Thromb. Vasc. Biol. 43, 92–108 (2023). [PubMed: 36412197]
53. Love MI, Huber W, Anders S, Moderated estimation of fold change and dispersion for RNA-seq data with DESeq2. Genome Biol. 15, 550 (2014). [PubMed: 25516281]
54. Wu T, Hu E, Xu S, Chen M, Guo P, Dai Z, Feng T, Zhou L, Tang W, Zhan L, Fu X, Liu S, Bo X, G., clusterProfiler 4.0: A universal enrichment tool for interpreting omics data. Innovation 2, 100141 (2021). [PubMed: 34557778]
55. Abdennur N, Mirny LA, Cooler: Scalable storage for Hi-C data and other genomically labeled arrays. Bioinformatics 36, 311–316 (2020). [PubMed: 31290943]
56. Serizay J, HiCool. R package version 1.4.0 (2023); https://github.com/js2264/HiCool.
57. Dixon JR, Jung I, Selvaraj S, Shen Y, Antosiewicz-Bourget JE, Lee AY, Ye Z, Kim A, Rajagopal N, Xie W, Diao Y, Liang J, Zhao H, Lobanenkov VV, Ecker JR, Thomson JA, Ren B, Chromatin architecture reorganization during stem cell differentiation. Nature 518, 331–336 (2015). [PubMed: 25693564]
58. Matthey-Doret C, Baudry L, Breuer A, Montagne R, Guiglielmoni N, Scolari V, Jean E, Campeas A, Chanut PH, Oriol E, Meot A, Politis L, Vigouroux A, Moreau P, Koszul R, Cournac A, Computer vision for pattern detection in chromosome contact maps. Nat. Commun. 11, 5795 (2020). [PubMed: 33199682]
59. Sarkar D, Gentleman R, Lawrence M, Yao Z, chipseq: A package for analyzing chipseq data. R package version 1.54.0 (2024).
60. Hahne F, Ivanek R, Visualizing genomic data using Gviz and Bioconductor. Methods Mol. Biol. 1418, 335–351 (2016). [PubMed: 27008022]
61. Van De Vlekkert D, Machado E, d'Azzo A, Analysis of generalized fibrosis in mouse tissue sections with masson's trichrome staining. Bio Protoc. 10, e3629 (2020).

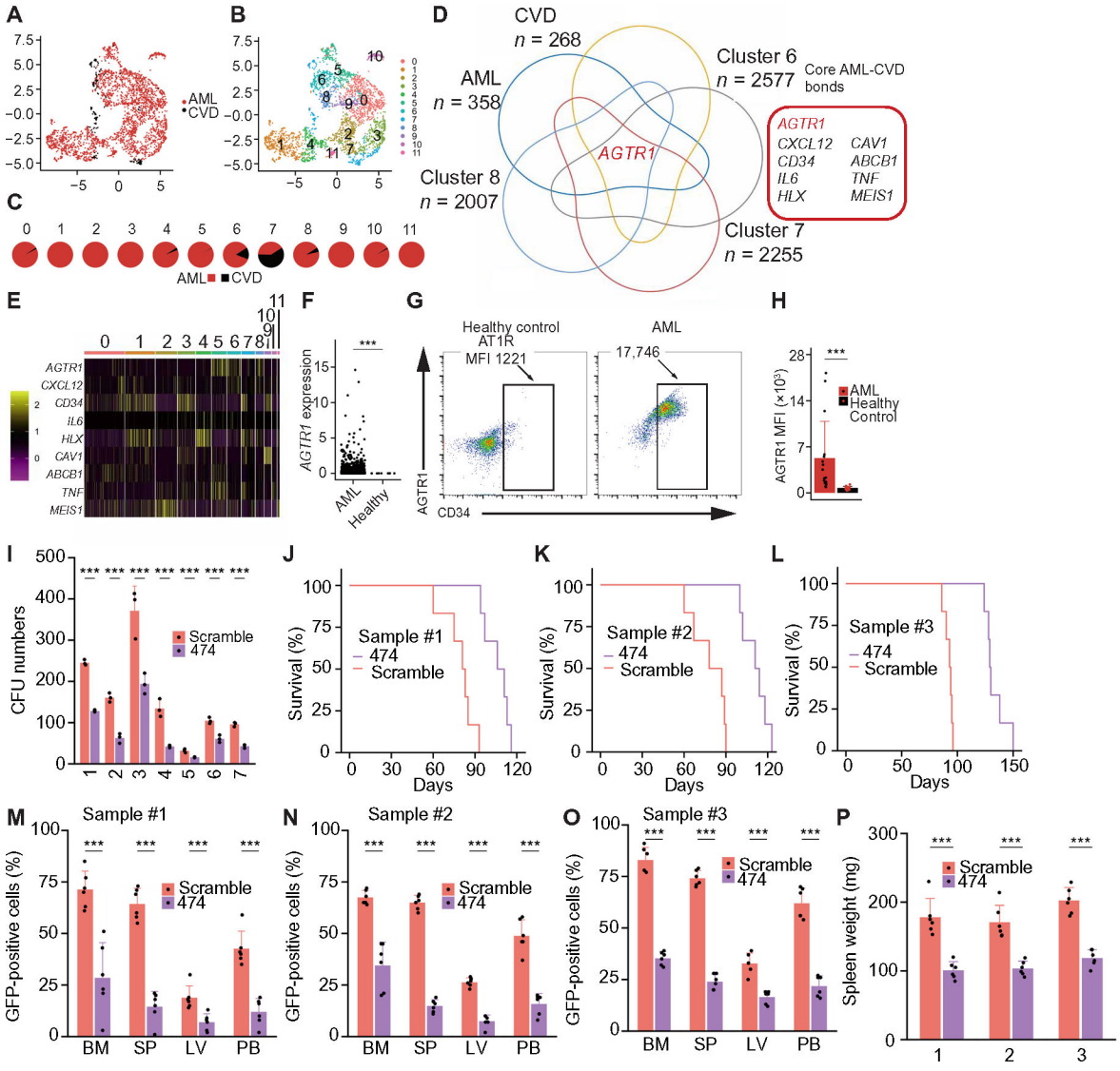

Fig. 1. AGTR1, a shared factor between AML and CVD, is essential for hAML development.

(**A**) Shown is a UMAP plot of patients with AML (red; $n = 2657$) and patients with CVD (black, $n = 176$). (**B**) Shown is a UMAP plot as in (A) colored according to the identified 12 clusters. (**C**) The pie charts show the relative distribution within each cluster by patients with AML and patients with CVD across the clusters. (**D**) The Venn diagram depicts the overlap between AML-related genes (identified from harmonizome, $n = 358$), CVD-related genes (identified from harmonizome, $n = 268$), and DEGs between each of clusters 6, 7, and 8, against clusters 1, 2, 3, 9, and 11. (**E**) The heatmap-related genes of AML/CVD identified through (D). Cell clusters are annotated at the top. (**F**) *AGTR1* gene expression in blood cells of patients with AML ($n = 706$) and of healthy control ($n = 15$) from BEATAML. Data are individual measurements. Student's *t* test, $^{***}P < 0.001$. (**G**) Representative flow cytometry plots are shown of the AGTR1 expression on cells of patients with AML and healthy control cord blood. Numbers above bracketed lines indicate the median fluorescence intensity (MFI) of the $CD34^{+}AGTR1^{+}$ cell population. (**H**) Quantification of (G) shows that

the comparison of AGTR1 MFI of $CD34^+$ cells in patients with AML ($n = 16$) and healthy control cord blood ($n = 12$) is shown. Student's t test, $^{***}P < 0.001$. (**I**) Shown is the comparison of CFU forming ability after *AGTR1*-KD in hAML cells from different patients (10,000 cells per well, $n = 3$ wells). x axis is hAML sample ID. Student's t test, $^{***}P < 0.001$. (**J**) Shown is the survival curve of hAML cell (patient #1)–transplanted NSG mice infected with scramble or sh*AGTR1*-474 virus ($n = 6$ mice). Log-rank test, $P < 0.0001$. (**K**) Shown is the survival curve of hAML cell (patient #2)–transplanted NSG mice infected with scramble or sh*AGTR1*-474 virus ($n = 6$ mice). Log-rank test, $P < 0.0001$. (**L**) Shown is the survival curve of hAML cell (patient #3)–transplanted NSG mice infected with scramble or sh*AGTR1*-474 virus ($n = 6$ mice). Log-rank test, $P < 0.0001$. (**M**) Shown is the summary (patient #1) of the proportions of GFP^+ cells in the BM, spleen (SP), liver (LV), and PB at day 120 after transplantation or when mice were euthanized ($n = 6$ mice). Student's t test, $^{***}P < 0.001$. (**N**) Shown is the summary (patient #2) of the proportions of GFP^+ cells in the BM, spleen, liver, and PB at day 120 after transplantation or when mice were euthanized ($n = 6$ mice). Student's t test, $^{***}P < 0.001$. (**O**) Shown is the summary (patient #3) of the proportions of GFP^+ cells in the BM, spleen, liver, and PB at day 120 after transplantation or when mice were euthanized ($n = 6$ mice). Student's t test, $^{***}P < 0.001$. (**P**) Bar plot shows the comparison of the weight of spleens of the mice transplanted with hAML cells expressing shRNA targeting *AGTR1* or scramble control ($n = 6$ mice). x axis is hAML sample ID. Student's t test, $^{***}P < 0.001$. Data are means + SD.

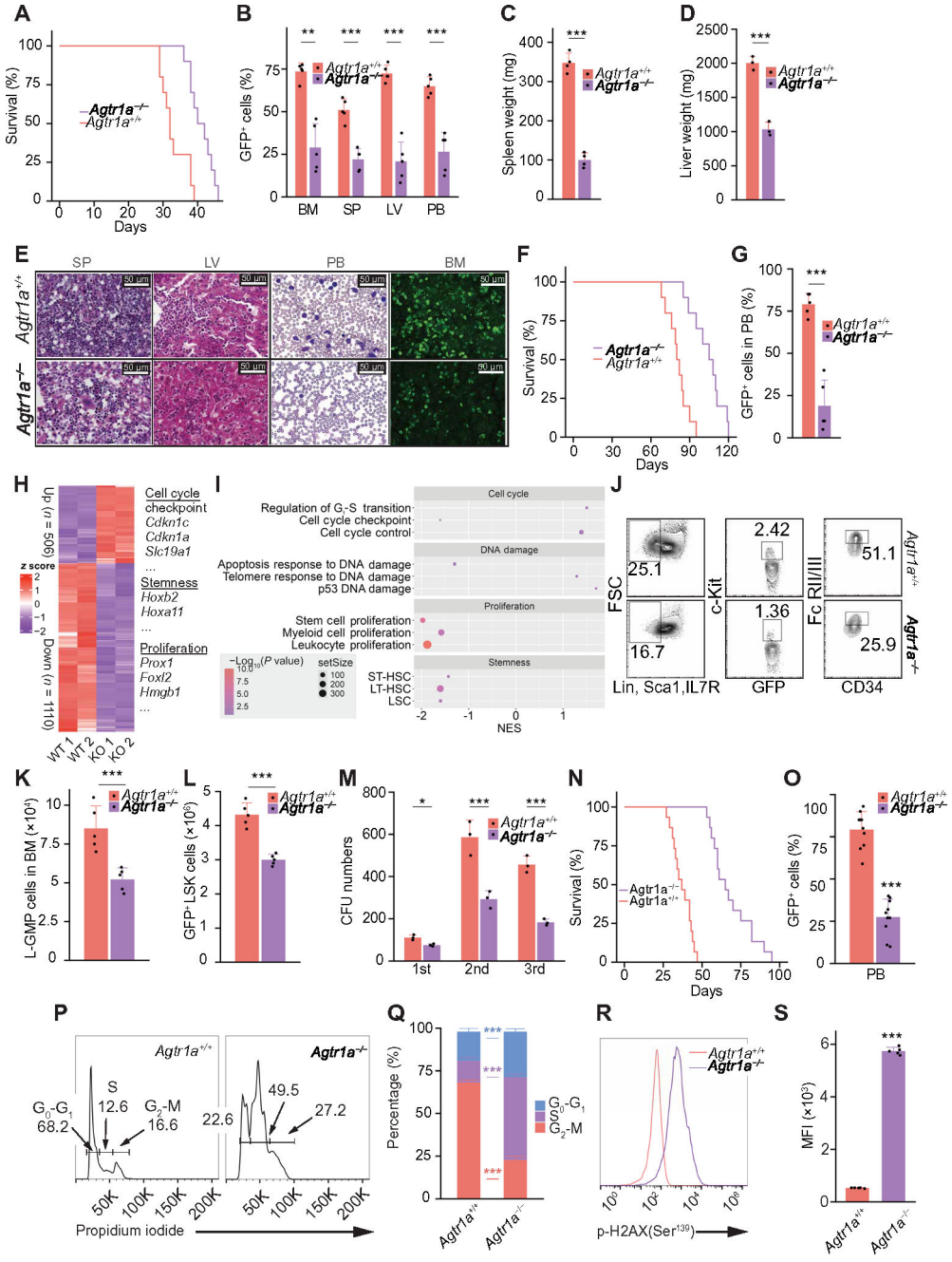

Fig. 2. *Agtr1a* KO reduces AML development through impaired LSC stemness in mice.

(**A**) Shown are the survival curves of mice receiving MLL-AF9 infected *Agtr1a*$^{+/+}$ and *Agtr1a*$^{-/-}$ HSPCs ($n = 10$ mice). Log-rank test, $P = 0.004$. (**B**) Shown is the comparison of the proportions of GFP^{+} AML cells in the BM, SP, LV, and PB of mice transplanted with *Agtr1a*$^{+/+}$ and *Agtr1a*$^{-/-}$ MLL-AF9 cells 4 weeks after transplantation ($n = 5$ mice). Student's *t* test, $^{**}P < 0.001$ and $^{***}P < 0.001$. (**C**) Shown is the SP weight of mice transplanted with *Agtr1a*$^{+/+}$ and *Agtr1a*$^{-/-}$ MLL-AF9 cells 4 weeks after transplantation ($n = 5$ mice). Student's *t* test, $^{***}P < 0.001$. (**D**) Shown is the LV weight of mice transplanted with *Agtr1a*$^{+/+}$ and *Agtr1a*$^{-/-}$ MLL-AF9 cells 4 weeks after transplantation ($n = 5$ mice).

Student's *t* test, ***$P < 0.001$. (**E**) Shown are the histological analysis of AML infiltration in the SP, LV, and PB and immunofluorescence analysis of the BM of mice 6 weeks after transplantation (hematoxylin and eosin staining for SP and LV, HEMA 3 staining for PB samples, and GFP that represents AML cells). Original magnification, ×600. Scale bars, 50 μm. (**F**) Shown are survival curves of mice receiving AML1-ETO9a–infected *Agtr1a*$^{+/+}$ and *Agtr1a*$^{-/-}$ HSPCs ($n = 10$ mice). Log-rank test, $P < 0.0001$. (**G**) Percentages of AML1-ETO9a GFP$^+$ leukemia cells in BM at 8 weeks after transplantation ($n = 5$ mice). Student's *t* test, ***$P < 0.001$. (**H**) RNA-seq analysis shows the DEGs (1.5 FC, $P < 0.05$) of *Agtr1a*$^{-/-}$ versus *Agtr1a*$^{+/+}$ MLL-AF9$^+$ AML cells ($n = 2$ groups). Genes of interest are highlighted. (**I**) Dot plot of gene set enrichment analysis (GSEA) results illustrates the biological processes associated with *Agtr1a* KO. *P* values are annotated with a colored scheme. NES, normalized enrichment score. (**J**) Representative of immunophenotypic analysis shows the AML stem cell (AML-SC) population [GMP-like leukemic cells (L-GMP, GFP$^+$Lin$^-$Sca-1$^-$IL7R$^-$Kit$^+$CD34$^+$FcγRII/III$^+$)] from the BM of *Agtr1a*$^{+/+}$ and *Agtr1a*$^{-/-}$ MLL-AF9 AML mice at moribund stage ($n = 5$ mice). (**K**) The bar plot shows absolute numbers of L-GMP in the BM of *Agtr1a*$^{+/+}$ and *Agtr1a*$^{-/-}$ MLL-AF9 AML mice at 6 weeks after transplantation ($n = 5$ mice). Student's *t* test, ***$P < 0.001$. (**L**) The bar plot shows absolute numbers of LSC (GFP$^+$Lin$^-$Sca1$^-$Kit$^+$) in the BM of mice transplanted with *Agtr1a*$^{+/+}$ or *Agtr1a*$^{-/-}$ AML1-ETO9a cells at 8 weeks after transplantation ($n = 5$ mice). Student's *t* test, ***$P < 0.001$. (**M**) Bar plot shows the comparison of CFU capability of *Agtr1a*$^{+/+}$ or *Agtr1a*$^{-/-}$ MLL-AF9 AML cells during serial plating (2000 cells per well, $n = 3$ wells). Student's *t* test, ***$P < 0.001$ and *$P < 0.05$. (**N**) Shown is the survival curve of secondary transplanted mice receiving 2000 *Agtr1a*$^{+/+}$ and *Agtr1a*$^{-/-}$ AML cells ($n = 15$ mice). Log-rank test, $P < 0.0001$. (**O**) Bar plot shows the proportion of GFP$^+$ AML cells in the PB of mice secondary transplanted with *Agtr1a*$^{+/+}$ or *Agtr1a*$^{-/-}$ AML cells at 4 weeks after transplantation ($n = 10$ mice). Student's *t* test, ***$P < 0.001$. (**P**) Representative flow cytometry analysis shows the cell cycle progression of *Agtr1a*$^{+/+}$ and *Agtr1a*$^{-/-}$ MLL-AF9 AML-SCs, stained with propidium iodide. Numbers above bracketed lines indicate the percentage of cells in phases G_0-G_1, S (middle), and G_2-M (right). (**Q**) Shown is the quantification of results in (J) ($n = 6$ mice), *Agtr1a*$^{-/-}$ versus *Agtr1a*$^{+/+}$, for G_0-G_1, S, and G_2-M. Student's *t* test, ***$P < 0.001$. (**R**) p-H2AX, phosphorylation of histone H2AX at Ser^{139} in *Agtr1a*$^{+/+}$ and *Agtr1a*$^{-/-}$ MLL-AF9 AML cells, is shown by flow cytometer. (**S**) Bar plot shows the MFI of p-H2AX in *Agtr1a*$^{+/+}$ and *Agtr1a*$^{-/-}$ MLL-AF9 AML cells. Data are means + SD. Student's *t* test, ***$P < 0.001$. Data are means + SD.

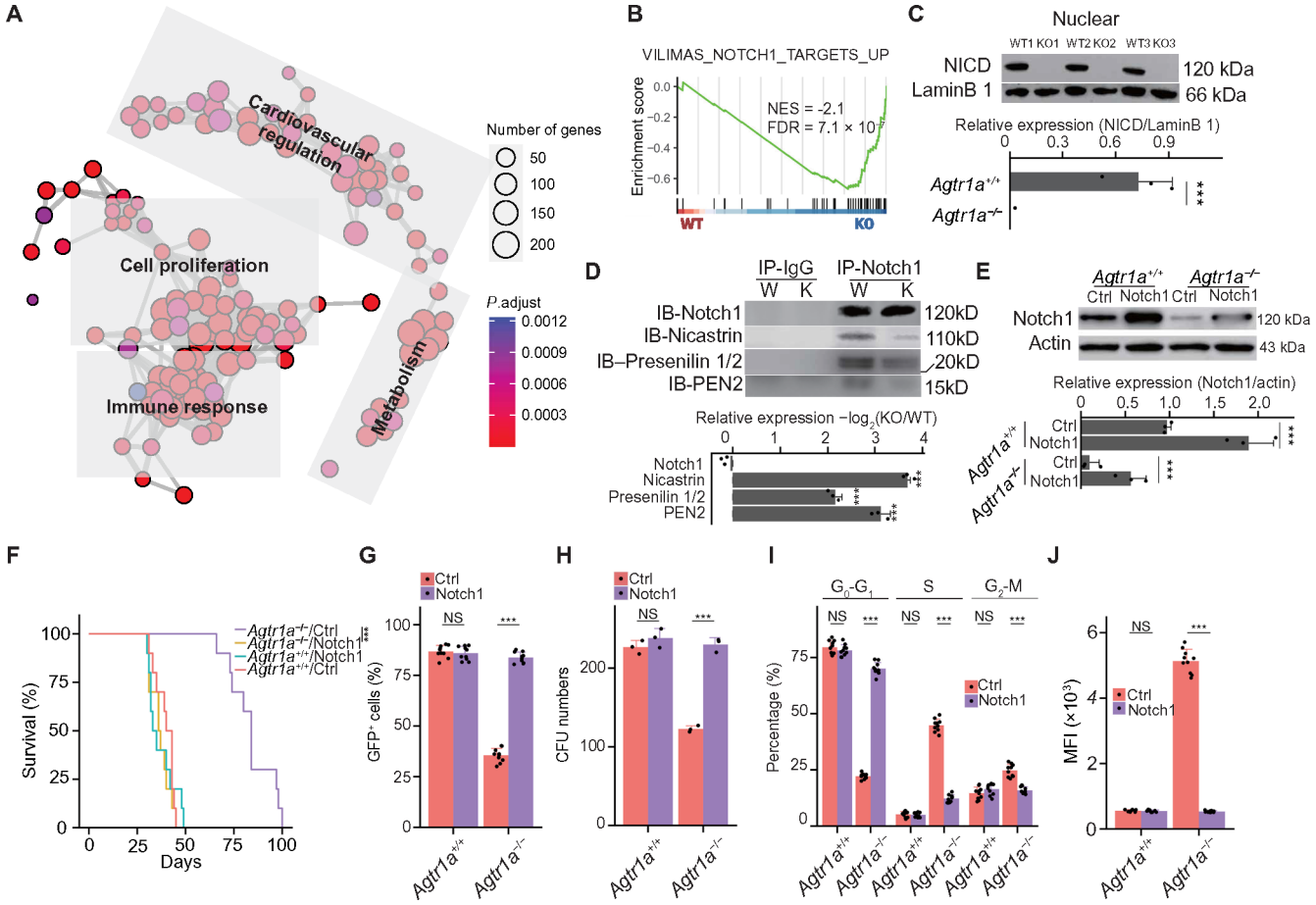

Fig. 3. Rescued Notch1 abrogates impaired AML cell stemness and cell division induced by *Agtr1a* KO in mice.

(**A**) Enrichment map analysis of leading edge shows significantly enriched pathways, including cardiovascular regulation, cell proliferation, immune response, and metabolism, in $Agtr1a^{-/-}$ compared with $Agtr1a^{+/+}$ AML cells. The length and thickness reflect the connectivity between each node. (**B**) GSEA plot shows significant down-regulation of Notch1 pathway gene signatures upon *Agt1ra* depletion. FDR, false discovery rate. (**C**) Shown is the comparison of NICD protein amounts using nuclei extracted from $Agtr1a^{-/-}$ (KO) and $Agtr1a^{+/+}$ (WT) MLL-AF9$^+$ BM cells of three primarily transplanted mice. Quantification of relative expression (NICD/LaminB 1) is shown by a bar plot at the lower panel ($n = 3$). Student's t test, $^{***}P < 0.001$. (**D**) Immunoblot (IB) analysis using Notch1 antibody shows Notch-binding native γ-secretase protein assemblies (nicastrin, presenilin 1/2, and PEN2). Quantification of relative expression scaled by immunoprecipitation (IP)–Notch1 is shown by a bar plot at the bottom panel ($n = 3$). Student's t test, $^{***}P < 0.001$. IgG, immunoglobulin G. (**E**) Western blot shows Notch1 expression after Notch1 or scramble overexpression in $Agtr1a^{+/+}$ and $Agtr1a^{-/-}$ MLL-AF9$^+$ BM cells. Quantification of relative expression (NICD/actin) is shown by a bar plot at the bottom panel ($n = 3$). Student's t test, $^{***}P < 0.001$. (**F**) Shown are the survival curves of mice transplanted with 2000 ectopically Notch1-expressing or control cells. $Agtr1a^{+/+}$ or $Agtr1a^{-/-}$ MLL-AF9$^+$ BM cells in primarily transplanted mice were collected at 40 days and were infected with

Notch1-encoding or control virus and transplanted into mice ($n = 10$ mice). Log-rank test, $***P < 0.001$. (**G**) Bar plot shows the proportions of GFP^+ AML cells in PB of secondary recipient mice after 28 days of transplantation ($n = 10$ mice). Student's t test, $***P < 0.001$; NS, $P > 0.05$. (**H**) Bar plot shows the colony-forming ability of *Agtr1a*$^{-/-}$ MLL-$AF9^+$ BM cells with reintroduction of Notch1 or infected with the control virus (2000 cells per well, $n = 3$ wells). Student's t test, $***P < 0.001$; NS, $P > 0.05$. (I) Bar plot shows Notch1 reintroduction rescued S phase arrest induced by *Agtr1a* KO in MLL-AF9 AML cells. Student's t test, $***P < 0.001$; NS, $P > 0.05$. (**J**) Bar plot shows the comparison of DNA damage in *Agtr1a* KO MLL-AF9 AML cells with or without Notch1 reintroduction. Student's t test, $***P < 0.001$. Data are means + SD.

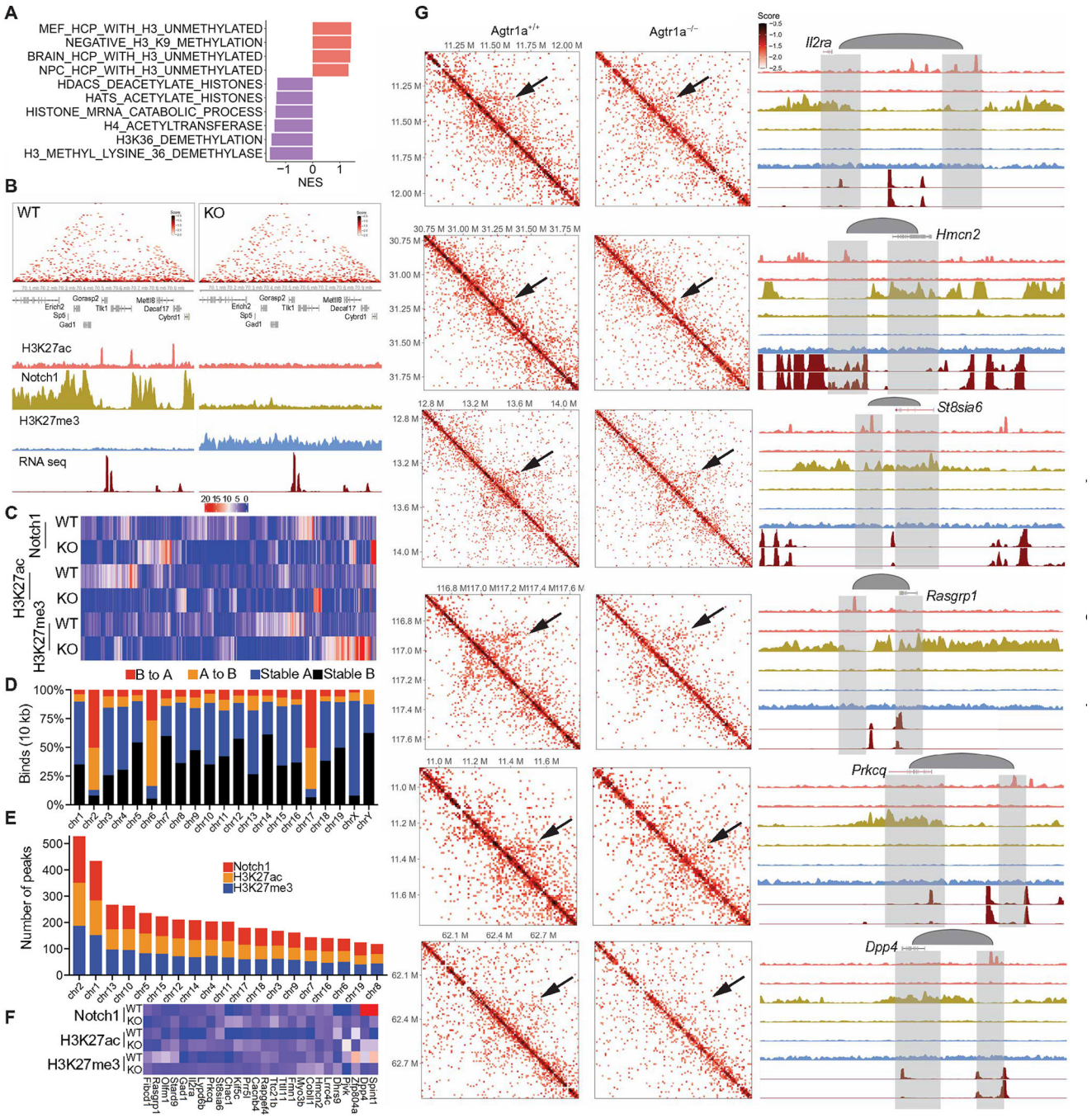

Fig. 4. AGTR1-Notch1 signaling regulates 3D genomic structure of chemoresistance genes.

(**A**) GSEA shows large-scale histone modification gene signatures change between *Agtr1a*$^{+/+}$ and *Agtr1a*$^{-/-}$ AML cells. (**B**) Snapshot of an example region shows Hi-C and CUT&RUN for H3K27ac, Notch1, H3K27me3, and RNA-seq data in the same region of a WT or KO mouse. Values for the *y* axis for the data were normalized to sequencing depths. (**C**) Heatmap shows DBGs of CUT&RUN between WT and *Agtr1a* KO MLL-AF9 AML. (**D**) Bar plot shows the proportion of A/B compartment switching in each chromosome after *Agtr1a* KO in MLL-AF9 AML. (**E**) Bar plot shows the number of differentially binding

sites on each chromosome in CUT&RUN data for Notch1, H3K27ac, and H3K27me3 after *Agtr1a* KO in MLL-AF9 AML. (**F**) Heatmap shows top DBGs between H3K27ac, Notch1, and H3K27me3. (**G**) Left shows Hi-C matrix surrounding of top DBGs identified in (F). Right, from top to bottom, shows the genome browser tracks for H3K27ac of *Agtr1a* WT and KO, Notch1 of *Agtr1a* WT and KO, H3K27me3 of *Agtr1a* WT and KO, and RNA-seq of *Agtr1a* WT and KO as a color scheme in (B). The gray arcs mark the loop anchors, which link the DBGs to distal enhancers.

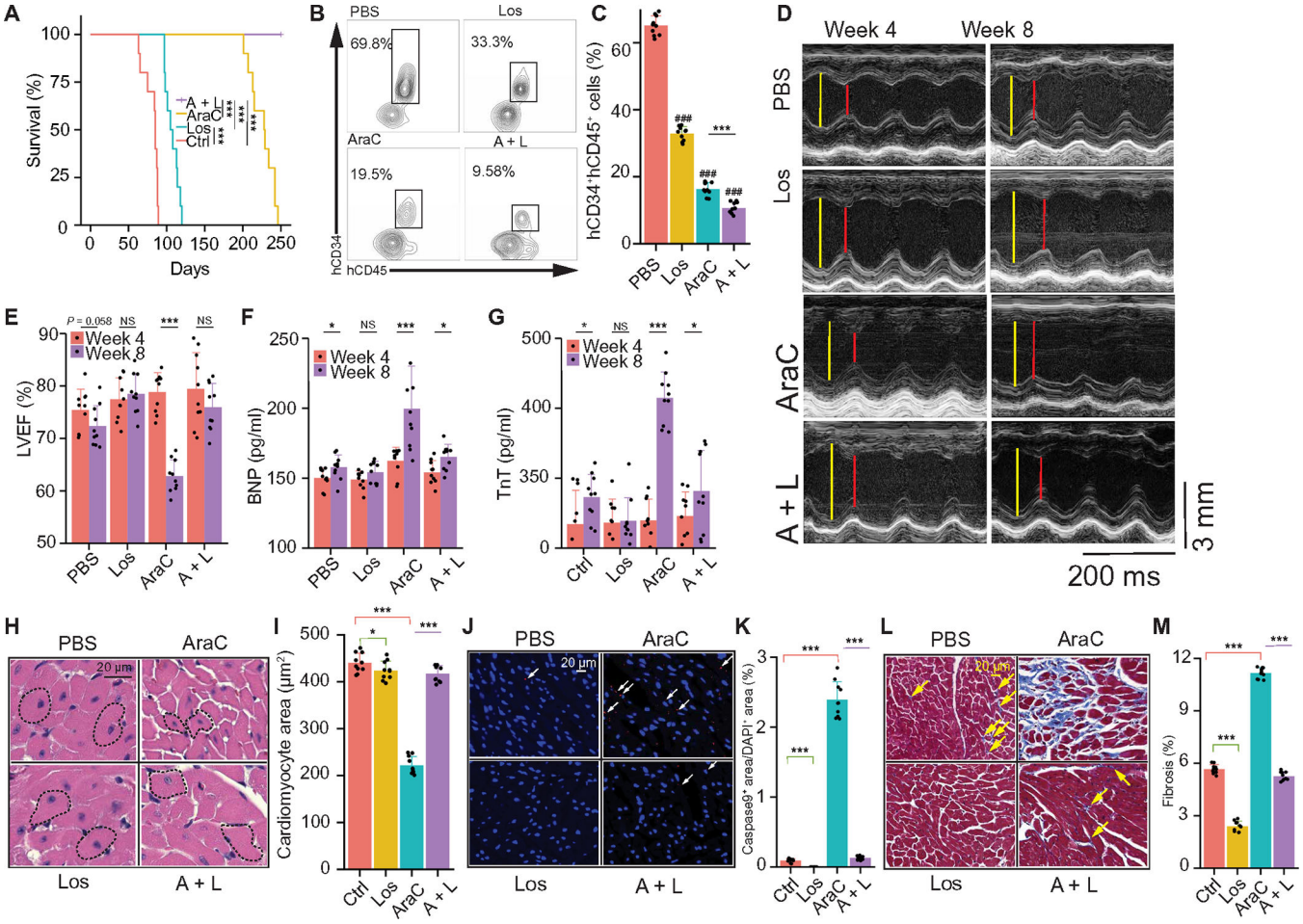

Fig. 5. An AGTR1 inhibitor simultaneously sensitizes AML to chemotherapy and relieves chemotherapy-induced cardiotoxicity.

(**A**) Shown are the survival curves of hAML-transplanted NSG mice treated by PBS, losartan, AraC, or losartan + AraC (treatment starts at 4 weeks after transplantation) ($n = 10$). Log-rank test, ***$P < 0.001$. (**B**) Shown is the representative flow cytometry analysis of $hCD34^+hCD45^+$ hAML cell percentage in PB of mice treated by PBS, losartan, AraC, or losartan + AraC. (**C**) Bar plot shows quantification of absolute numbers of the $hCD34^+hCD45^+$ hAML cell percentage in PB of mice treated by PBS, losartan, AraC, or losartan + AraC ($n = 10$ mice). Student's t test, ***$P < 0.001$ and $^{###}P < 0.001$ compared with PBS. (**D**) Shown are the representative M-mode echocardiographic images of hearts of mice treated by PBS, losartan, AraC, or losartan + AraC 4 and 8 weeks after transplantation. Yellow and red lines indicate left ventricular end-diastolic diameter and left ventricular end-systolic diameter, respectively. Scale bars, 200 ms, 3 mm. (**E**) Bar plot shows LVEF of hearts of mice treated by PBS, losartan, AraC, or losartan + AraC ($n = 10$) 4 and 8 weeks after transplantation. Student's t test, ***$P < 0.001$; NS, $P > 0.05$. (**F**) Bar plot shows plasma BNP amount of mice treated by PBS, losartan, AraC, or losartan + AraC ($n = 10$) 4 and 8 weeks after transplantation. Student's t test, ***$P < 0.001$. (**G**) Bar plot shows plasma troponin T (TnT) amount of mice treated by PBS, losartan, AraC, or losartan + AraC ($n = 10$) 4 and 8 weeks after transplantation. Student's t test, *$P < 0.05$; ***$P < 0.001$;

NS, $P > 0.05$. (**H**) Shown are the representative images of hematoxylin and eosin (×600) staining of cardiomyocyte area in heart sections from mice treated in by PBS, losartan, AraC, or losartan + AraC. Scale bar, 20 μm. (**I**) Bar plot shows the relative quantification of cardiomyocyte area in heart sections from mice treated in by PBS, losartan, AraC, or losartan + AraC ($n = 10$ mice). Student's t test, $^{*}P < 0.05$ and $^{***}P < 0.001$. (**J**) Shown are the representative images of caspase-9 staining in heart sections from mice treated by PBS, losartan, AraC, or losartan + AraC. The arrow denotes caspase-9 positive sites. Scale bar, 20 μm. (**K**) Bar plot shows relative quantification of caspase-9 staining in heart sections from mice treated by PBS, losartan, AraC, or losartan + AraC ($n = 10$ mice). Student's t test, $^{***}P < 0.001$. DAPI, 4′,6-diamidino-2-phenylindole. (**L**) Shown are the representative images of trichrome staining (×200) of heart sections from mice treated by PBS, losartan, AraC, or losartan + AraC. The arrow denotes fibrotic sites. (**M**) Bar plot shows the relative quantification of trichrome staining in heart sections from mice treated by PBS, losartan, AraC, or losartan + AraC ($n = 10$ mice). Student's t test, $^{***}P < 0.001$. Data are means + SD.

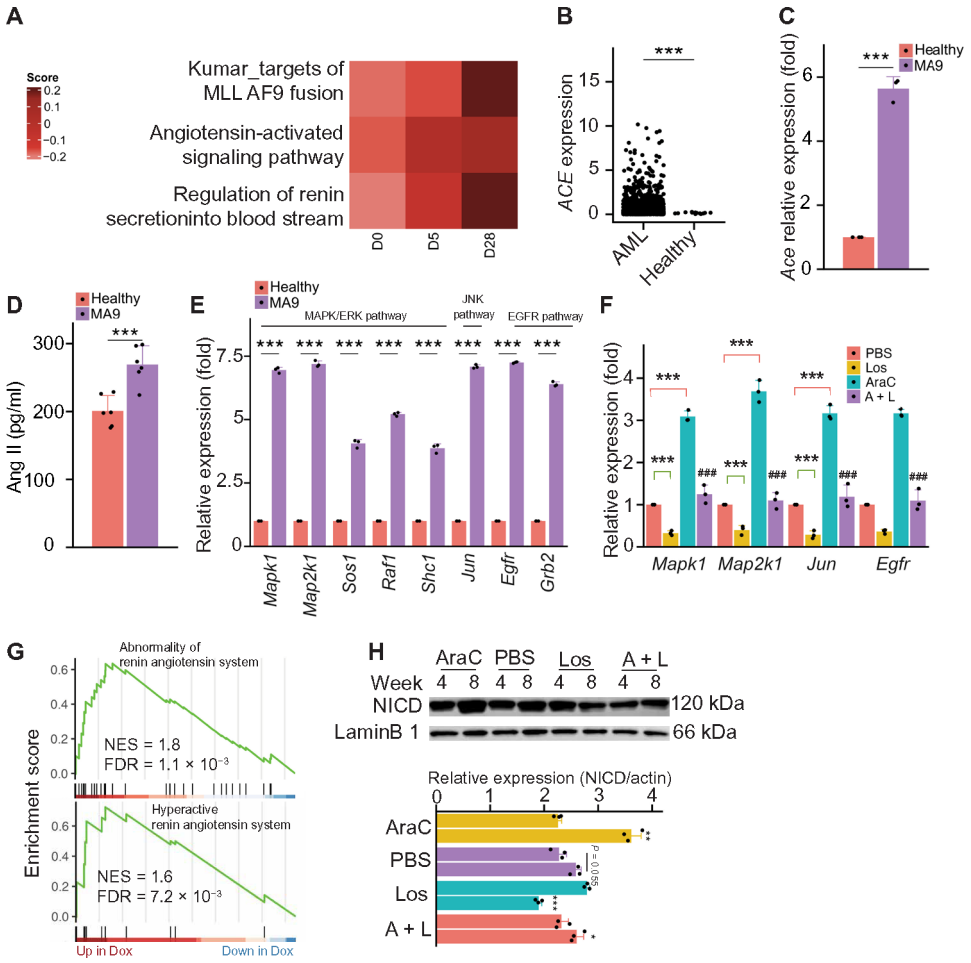

Fig. 6. AGTR1 activation associates AML- and chemotherapy-induced cardiomyocyte toxicity.

(**A**) Heatmap depicts the ssGSEA projection of MA9 gene set and angiotensin gene sets on day 0 (D0), day 5 (D5), and day 28 (D28) after MA9 introduction. (**B**) Bar plot shows *ACE* gene expression in blood cells of patients with AML ($n = 706$) and of healthy control ($n = 15$) from BEATAML. Student's t test, $^{***}P < 0.001$. Data are individual observations. (**C**) Bar plot shows the quantitative real-time polymerase chain reaction (PCR) analysis of the expression of *Ace* mRNA in AML cells isolated from healthy or MLL-AF9 mice BM ($n = 3$ mice per group), presented relative to expression by healthy cells. Student's t test, $^{***}P < 0.001$. (**D**) Bar plot shows the plasma angiotensin II (Ang II) amount of healthy or MLL-AF9 mice 4 weeks after transplantation ($n = 6$ mice per group). Student's t test, $^{***}P < 0.001$. (**E**) Bar plot show the quantitative real-time PCR analysis of the expression of transcripts encoding AGTR1 downstream genes *Mapk1*, *Map2k1*, *Sos1*, *Raf1*, *Shc1*, *Jun*, *Egfr*, and *Grb2* in hearts isolated from healthy or AML mice 4 weeks after transplantation ($n = 3$ mice per group), presented relative to expression by healthy mice. Student's t test, $^{***}P < 0.001$. (**F**) Bar plot show the quantitative real-time PCR analysis of *Mapk1*, *Map2k1*, *Jun*, and *Egfr* in hearts of mice treated by PBS, losartan, AraC, or losartan + AraC ($n = 3$ mice per group), presented relative to expression by healthy mice. Student's t test, $^{***}P < 0.001$ and $^{\#\#\#}P < 0.001$ when compared with AraC. (**G**) GSEA plot shows activated angiotensin pathway gene signatures in doxorubicin-treated cardiomyocytes. Data are from Schwach *et*

al. (51), GSE232331. (**H**) Western blot shows NICD expression in hearts of mice treated by PBS, losartan, AraC, or losartan + AraC ($n = 3$). Student's t test, $^{*}P < 0.05$, $^{**}P < 0.01$, and $^{***}P < 0.001$.